6 ECA 18 Temporal Decay

6.1 Hamming Vicinity Decay

Returning now to our investigation of the stability ECA 18's attractors, we study the temporal relaxation of the Hamming vicinity back onto the attractor in relation to the stochastic decay models. As discussed above, the Hamming vicinity is the physically realistic vicinity to use, since it traces the response of the system to spatially local perturbations.

Hamming vicinity decay for ECA 18 was investigated for a number of lattice sizes $N < 1000$, largely chosen arbitrarily. For each lattice, an initial vicinity ensemble was created as described in Sec. 4. At each time step each pattern in the ensemble was iterated once. The number of dislocations was counted using the method described in Ref. [8]. When the number fell below two, that pattern was removed from the ensemble, since it was on the attractor. States with two or more dislocations were allowed to continue evolving until their dislocations annihilated or they were proven to be on a periodic orbit. The latter condition was detected using a method described in Ref. [18]. At each time, the fraction $f_\Lambda(t)$ of states on the attractor was measured, and the nonattracted fraction $f_P(t)$ was calculated according to $f_P(t) = 1 - f_\Lambda(t)$. Vicinity ensemble sizes of $M_1 = 2 \times 10^4$, $M_2 = 1 \times 10^5$, and $M_3 = 1 \times 10^6$ were used. For $N > 500$ the ensembles were all of the size M_1; otherwise the size was chosen arbitrarily between M_2 and M_3, and appeared to have little effect on the results, other than reducing statistical fluctuations in the estimated fractions at large times.

We investigated 12 lattice sizes selected to be in the following groups.

1. Worst case.[8,19] The lattices with the largest asymptotic fraction f_P are those with $N_k = 3 \cdot 2^k - 2, k = 0, 1, 2, \ldots$. The difference in size between lattices in this set grows exponentially; we call such sets "sparse". We chose the subset $N_{wc} = \{22, 46, 94, 190, 382, 766\}$.
2. Winding number $\omega = 0$. The winding number ω is the "rotation rate" of spatial patterns on temporally periodic orbits of a finite lattice.[12] Since the nonattracted orbits in the vicinity are all temporally periodic, we initially hypothesized that the winding number might affect the statistics of vicinity convergence. Of the lattices with $\omega = 0$ we chose the subset $N \in \{20, 24, 36\}$.
3. Winding number $\omega = 1$: $N \in \{14, 31, 42\}$.

In addition to the above groups, we collected the same statistics on a larger set of 22 arbitrarily selected lattice sizes: even lattices $N_e = \{32, 34, 66, 178, 530, 536, 598, 790, 840, 880\}$ and odd lattices $N_o = \{27, 45, 77, 95, 99, 213, 629, 693, 781, 799, 879, 919\}$.

Not surprisingly, the decay profiles $f_P(t)$ for even-size lattices showed a characteristic shape different from that of N odd. We label these two classes (I) even-N, and (II) odd-N. In addition, the even-N lattices fell into two distinct subclasses: (IA) decelerating-decay and (IB) catastrophic-decay. Classes IA, IB, and II are shown respectively in Figs. 4, 5, and 6.

All of the even-N lattices follow a common backbone for the early part of their evolution. This backbone closely follows the stochastic RCW decay profile $f_{RCW}(t)$; the latter is plotted as a dashed line in all three figures. For example, in Fig. 4, the backbone appears as a solid curve lying just below the dashed RCW curve. The time-1 fraction $f_P(1)$ is the same for all lattices in classes IA and IB, but differs from $f_{RCW}(1)$ by 15%. In addition, the random cliff walker decays slightly more quickly than the ECA 18 backbone, so that the difference between the two grows less with time. Lattices in class IA remain on the backbone until they approach their asymptotic values. In class IB, each lattice shows a marked downturn away from the backbone before convergence. For nearly all of these catastrophic-decay lattices (with exceptions noted below), this downturn coincides with the RMW's transition to its second (exponential) decay epoch. The convergence of the curves to nonzero values of $f_P(t)$, in Fig. 4 and subsequent figures, is due to periodic orbits in the vicinity that do not fall back into the attractor. The RCW and RMW models do not capture such structure, and so $f_{RCW}(t)$ and $f_{RMW}(t)$ continue to decay indefinitely.

The lattices in class IA, the decelerating-decay class, were

$$N \in \{20, 22, 32, 34, 42, 46, 66, 94, 190, 382, 766\} \tag{13}$$

Figure 4 shows a log-log plot of the nonattracted fraction $f_P(t)$ vs. t for these lattices. Lattices in this class follow the common backbone of class I lattices for nearly all of their evolution. Near the convergence time T_c there is a gentle leveling as the decay curve makes its final approach to a nonzero asymptotic value. In the figure, the curves have been plotted up to $t = 2T_c$ to show the values of f_P. Within the overall class, T_c appears to be roughly proportional to lattice size, and so f_P approaches 0 in the limit of large N. The worst-case lattices N_{wc}, whose asymptotic nonattracted fractions are maximal, fall into the decelerating-decay class.

This class can be characterized as having early convergence, since T_c of each lattice is less than the RMW transition time T_d. The asymptotic fraction is reached before the transition to the second stochastic epoch can occur. For lattices in class IA, the evolution begins to diverge from the stochastic model only during the final approach to the asymptotic limit.

Figure 5 shows $f_P(t)$ for class IB, catastrophic decay. The lattices shown are

$$N \in \{14, 24, 36, 62, 178, 530, 536, 598, 790, 840, 880\} \tag{14}$$

As for class IA, $f_P(t)$ for these lattices initially follows the even-N backbone. At some point there is a transition to a markedly higher decay rate as seen in the profiles' downturn, which continues up to the convergence time. The time at which the transition occurs is within a few per cent of the RMW transition time T_d on larger lattices, and within a factor of 2 on the smaller

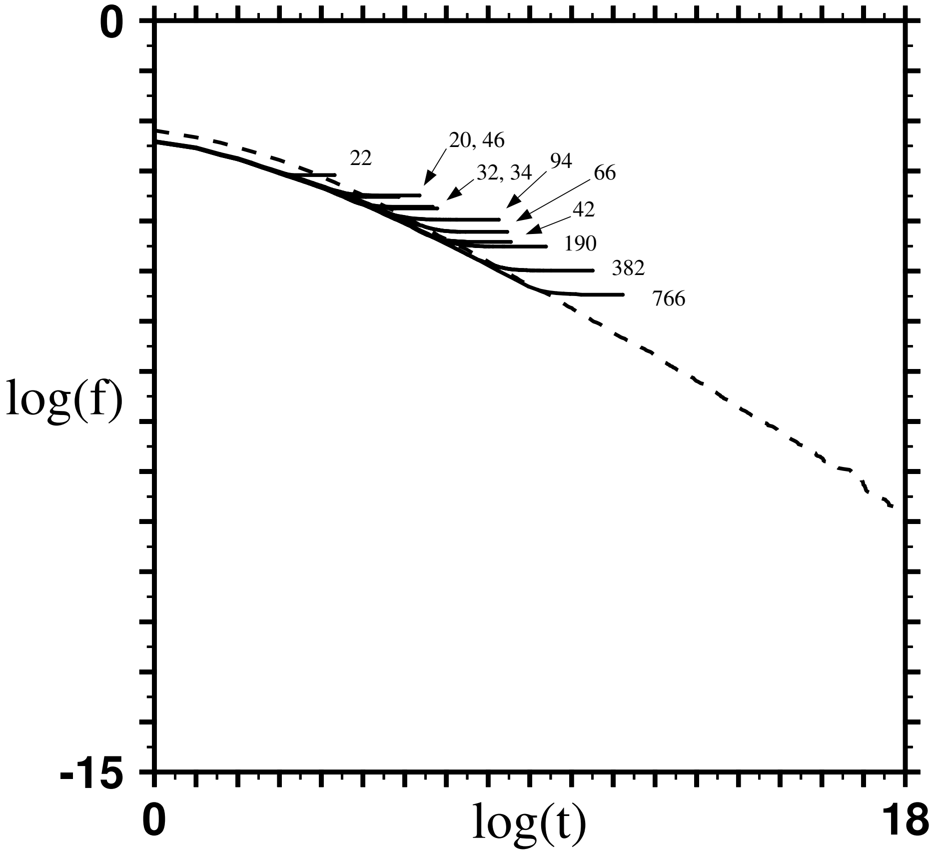

Fig. 4. Decelerating decay (class IA): $f_P(t)$ for lattice sizes $N \in \{20, 22, 32, 34, 42, 46, 66, 94, 190, 382, 766\}$. All curves are labelled by lattice size and plotted to $t = 2T_c$. For reference the dashed line gives the rescaled random cliff walker decay $f_{RCW}(t)$.

ones. The asymptotic nonattracted fraction f_P can be zero or a finite value. As for class IA, the lattices with nonzero f_P are indicated by horizontal tails extending to $t = 2T_c$. The three rightmost curves, $N \in \{790, 840, 880\}$, were still decaying when the evolution was stopped at $t = 240,000$. The remaining curves have $f_P = 0$, and are plotted to $t = T_c - 1$.

Two exceptional lattices, $N \in \{14, 62\}$, are included in the catastrophic-decay class, even though they converge before the RMW transition time T_d for those lattices. These are the leftmost two downward-pointing curves in Fig. 5. These lattices are members of the sparse set for which all states in the vicinity evolve to the null state 0^*. These lattices have size $N = 2^k - 2,\ k = 2, 3, ...$ Since the null state is in the attractor, $f_P = 0$ for these lattices. The sharp downturn in these curves is due to the sudden decay to 0^* at time $T_c = (N + 2)/2$.

Superimposed on the decay curve for $N = 178$ is the random mesa walker decay profile $f_{RMW}(t)$ for that lattice size. It is shown as the dashed line leading off the bottom of the plot.

The agreement between the two curves is remarkable; they overlap nearly all the way to T_c. This is typical of the larger class IB lattices. Smaller lattices tend to diverge from the corresponding RMW curves before T_c. As for class IA, typical lattices in class IB closely agree with the RMW stochastic model for nearly all of their evolution.

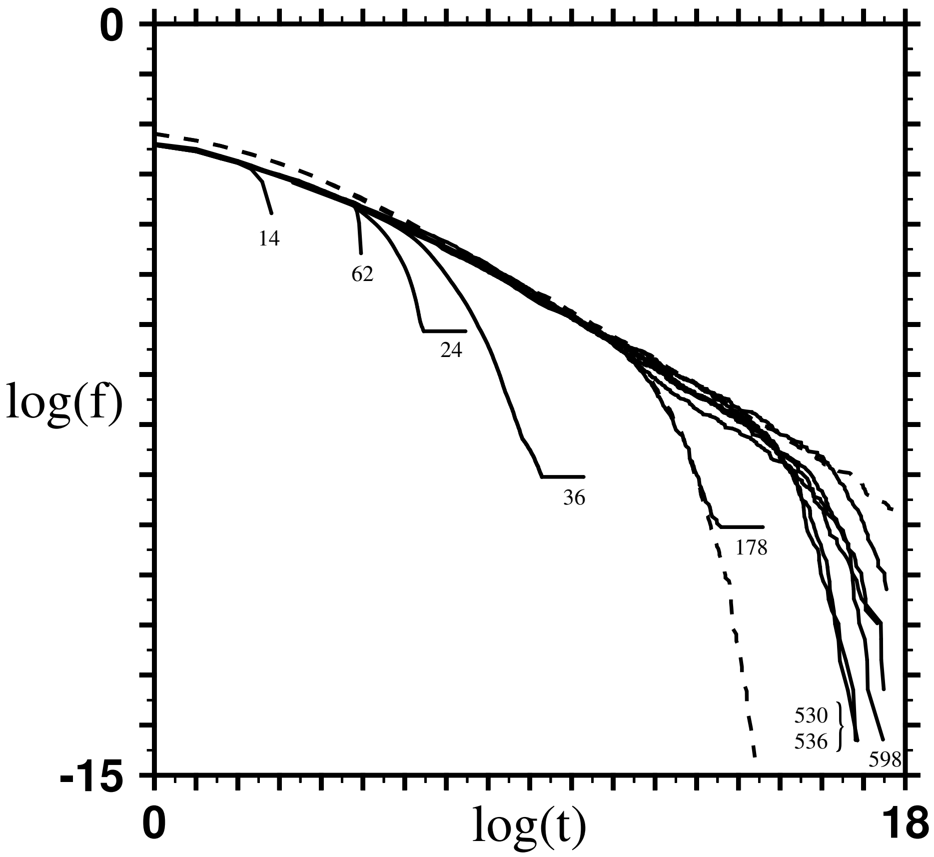

Fig. 5. Catastrophic decay (class IB): $f_P(t)$ for lattice sizes $N \in \{14,\ 24,\ 36,\ 62,\ 178,\ 530,\ 536,\ 598,\ 790,\ 840,\ 880\}$. Curves for all but the largest three rightmost curves are labelled by lattice size. Lattices $N \in \{24, 36, 178\}$ have nonzero f_P and are plotted to $t = 2T_c$. The three rightmost curves, from top to bottom $N \in \{840, 790, 880\}$, are plotted to the cutoff time $t = 240,000$. The remaining curves have $f_P = 0$ and are plotted to $t = T_c - 1$. For reference the upper dashed line gives the random cliff walker decay $f_{RCW}(t)$. In addition, the random mesa walker decay profile for $N = 178$ is shown as the dashed line leading off the bottom of the figure.

The odd-size, class II, lattices

$$N \in \{27,\ 31,\ 45,\ 77,\ 95,\ 99,\ 213,\ 629,\ 693,\ 781,\ 799,\ 879,\ 919\} \tag{15}$$

plotted in Fig. 6, show the same downward curve as the decelerating decay class, except that they appear to decay more quickly than even lattices of similar size. Some of the lattices have overlapping $f_P(t)$; for example, $N \in \{95, 99\}$ lie atop one another until the latter converges to $f_P = 0.0035$, and the lattices $N \in \{629, 693, 781, 799\}$ overlap throughout their evolution. Those lattices with nonzero f_P are plotted with horizontal tails to $t = 2T_c$, as for classes IA and IB; all others have $f_P = 0$.

The time-1 fraction $f_P(1)$ varies with lattice size with roughly the same form as for the 2D RMW, i.e., $f_P(1) \approx c_1 - c_2/N$, with $c_1 \approx 0.19$, $c_2 \approx 1.2$. However, $f_P(1) < f_{RMW}(1)$ for all lattices; in this, class II is similar to class I. In general, comparison with the 2D RMW decay curves shows that most lattices follow in parallel with the stochastic-model profiles, differing from them by a roughly constant factor. A typical lattice showing this effect is $N = 213$, for which $f_{RMW}(t)$ is plotted in Fig. 6 as a dashed line leading off the bottom of the figure. The ECA 18 decay curve for $N = 213$ runs parallel to it until the final approach to the asymptotic fraction. For some lattices, e.g. $N \in \{95, 99\}$, the agreement between $f_P(t)$ and $f_{RMW}(t)$ is nearly perfect.

In summary, then, the Hamming vicinity decay profiles agree well with the appropriate random mesa walker model, up until they reach the final approach to the asymptotic value f_P. The agreement is increasingly good for larger N. Even-size lattices differ primarily in whether this limit is reached before or after the transition to the second (exponential) epoch of RMW decay. For decelerating-decay (class IA), the convergence time T_c is less than the RMW transition time T_d, and the asymptotic fraction f_P is nonzero. For catastrophic-decay (class IB) $T_c > T_d$, and f_P is very small or zero. On odd-size lattices, the quantitative agreement with the stochastic model is less good, although the 2D RMW does capture the shapes of the decay curves.

The fact that the decay profiles fall into only a few classes gives some hope to simply describing the geometry of the discrete state space using the qualitative dynamics of Ref. [8] in conjunction with statistical methods. We sketch the beginnings of such a description here; a detailed analysis will require connecting the discrete state space view with the qualitative dynamics analysis we have used. Recall the discussion at the end of Sec. 4 above, which indicated that the convergence time T_c is equal to the length of the longest transient starting in the vicinity, and the instantaneous decay rate $\Delta f_P(t)$ is the same as the probability density of transient lengths. Applying this to the observed decay profiles of the three classes, we see from the convergence times T_c that lattices in class IA have relatively short transients, while for classes IB and II, there exist transients that are much longer: for example, compared to the class IA lattice $N = 766$, class IB lattice $N = 790$ and class II lattice $N = 781$ have transients that are about 500 and 100 times longer, respectively. For all lattices, linear plots of $f_P(t)$ vs. t show that $\Delta f_P(t)$ decreases quickly to zero with t. This is especially true of lattices in classes IB and II, for which $\Delta f_P(t)$ decreases exponentially during the second epoch of their evolution. Thus the distribution of transient lengths is sharply peaked at small values; there are many more short transients than long ones. Furthermore, the close agreement between the Hamming vicinity decay and the random mesa walker profiles shows that for each of classes

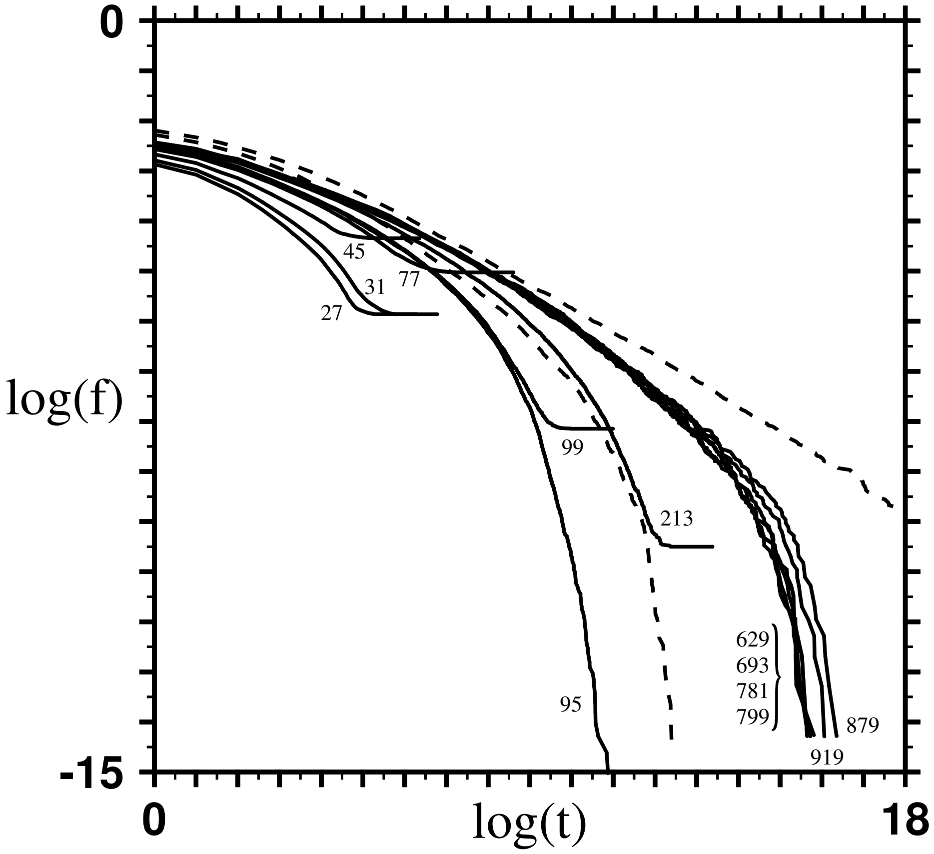

Fig. 6. Odd-N (class II): $f_P(t)$ for lattice sizes $N \in \{27, 31, 45, 77, 95, 99, 213, 629, 693, 781, 799, 879, 919\}$. All curves are labelled by lattice size. Lattices with nonzero f_P are plotted to $t = 2T_c$; all others are plotted to $t = T_c - 1$. The dashed line lying above all of the decay profiles is the random cliff walker decay $f_{RCW}(t)$. The 2D RMW curve for $N = 213$ is visible as a dashed line curving downward toward the bottom of the plot.

I and II, the distribution of transient lengths up to the cutoff at T_c is well-approximated by a single family of functions parametrized by N.

To get at the large-N, long-time behavior, we observe that the asymptotic fractions f_P are maximal on a sparse set N_{wc} of lattices, and even within this set appear to decrease with lattice size as $f_P \propto N^{-1/2}$.[8,19] Beneath this upper bound, f_P fluctuates wildly with N, indicating sensitivity to the number-theoretic properties of the lattice size. The dependence of f_P on N is exactly the type of question the algebraic analysis should answer; we plan to discuss this in greater detail in the future.

Finally, the decay profiles did not indicate any great dependence on lattice winding number ω, except that $\omega = 0$ lattices decay more rapidly than comparable $\omega = 1$ lattices.

6.2 Noisy Lattices

As a second method of examining the typical behavior of ECA 18, we added a small amount of random noise to the iteration rule. The extent to which this affects the vicinity convergence profile $f_P(t)$ gives an indication of the stability of the orbits under this perturbation: in particular, of the periodic orbits off the attractor.

The random noise took a particular form, chosen specifically to be the "minimal" perturbation to a state in the vicinity. At each time step, domain wild-card cells are flipped with i.i.d. probability p_{flip}. The latter is set so that approximately one cell in the lattice is flipped per iteration, i.e., $p_{flip} \approx 2/N$ since there are approximately $N/2$ wild-card cells in a vicinity state. This perturbation does not change the number or the positions of the dislocations. Instead it addresses the questions of whether such a weak perturbation is sufficient to destroy the nonattracted periodic orbits, or whether they are stable, i.e., whether they are themselves attractors.

The overall expectation is that the noise should not affect the decay behavior in the early diffusive epoch. During the later epoch, when the statistics of the noise-free evolution are dominated by the periodic orbits, the stability of those orbits will determine the effect of the noise. If the periodic orbits are unstable, then the asymptotic fraction f_P should decay to zero. Furthermore, the differences in the shape of $f_P(t)$ for different lattices sizes should be less pronounced.

We gathered statistics for ten lattices $N \in \{31, 36, 42, 45, 66, 94, 190, 213, 536, 693\}$ using ensembles of size $M = 1 \times 10^4$. This group includes examples of all three decay classes defined above. $f_P(t)$ is plotted for these lattices in Fig. 7. Lattices $N \in \{536, 693\}$ are plotted to $t = 30,000$; all others are plotted to $T_c - 1$. The results can be summarized as follows.

The two largest lattices, $N \in \{536, 693\}$ were still decaying when the evolution was stopped at $t = 30,000$; since both of these lattices have $f_P = 0$ for the unperturbed case, we expect the noisy decay to have zero asymptotic value as well. On all other lattices, $f_P(t)$ decayed to zero at finite t. There was no levelling off to a nonzero asymptotic value; the decay profiles for all lattices followed the appropriate RMW curve all the way to $f_P = 0$. This difference is most significant in the case of the decelerating-decay (class IA) lattices $N \in \{42, 66, 94, 190\}$, two of which are in the worst-case set N_{wc}. These lattices actually took on the catastrophic profile of class IB. The RMW decay profile $f_{RMW}(t)$ for the worst-case lattice $N = 190$, plotted in Fig. 7 as the dashed line curving down off the edge of the figure, shows a roughly constant offset from the noisy decay profile $f_P(t)$; there is no trace of the decelerating-decay behavior of the noise-free evolution. Neither the catastrophic-decay (class IB) lattices $N \in \{36, 536\}$ nor the odd-N (class II) lattices $N \in \{31, 45, 213, 693\}$ were significantly affected, up to the time when the unperturbed decay began to level off.

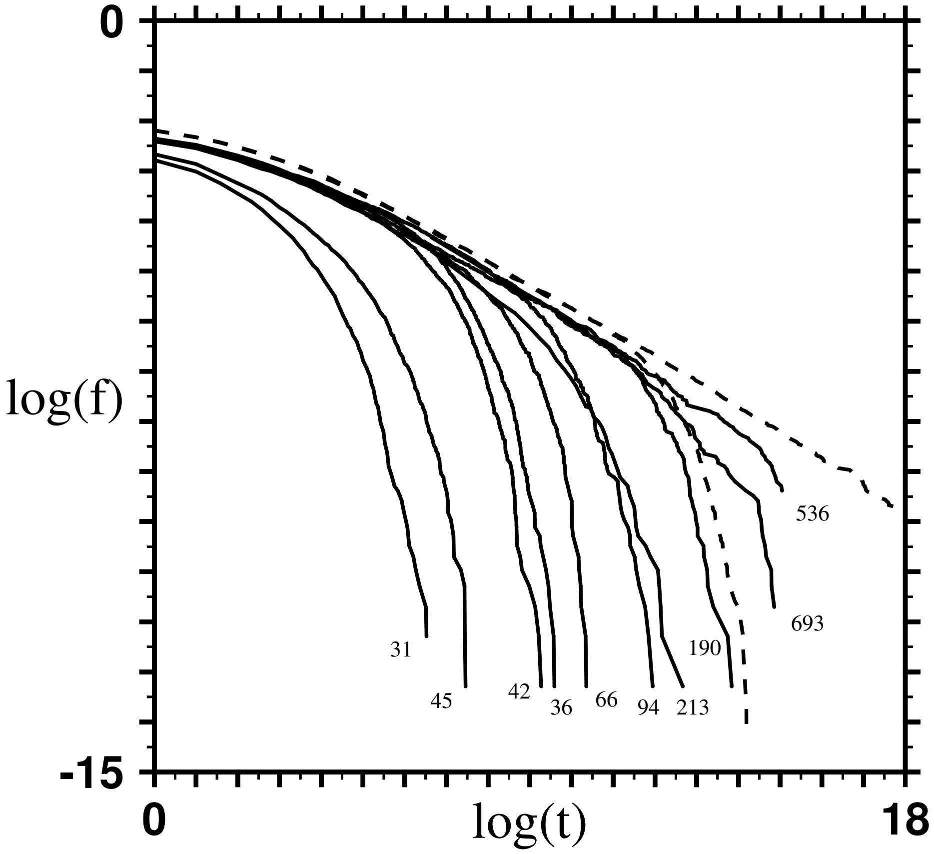

Fig. 7. The effect of noise: $f_P(t)$ vs. t for representative lattices $N \in \{31, 36, 42, 45, 66, 94, 190, 213, 536, 693\}$ from each class, with minimal stochastic perturbations in the domains. All curves are labelled by lattice size. Lattices $N \in \{536, 693\}$ were halted at $t = 30,000$ before they reached their asymptotic values; all other lattices decayed to $f_P = 0$ and are plotted to $t = T_c - 1$. As before, $f_{RCW}(t)$ is shown as a dashed line. The RMW decay curve for lattice $N = 190$, which is in the decelerating-decay class for noise-free evolution, is also shown as the dashed line curving down off the bottom of the page.

We interpret these results to indicate that the periodic orbits nearby, but not in, the attractors Λ^0 and $\Lambda^{0,0}$ are unstable to small perturbations. The detailed orbit structure imposed by the number-theoretic properties of the lattice size N is washed out by weak noise. Thus, the set of asymptotically nonattracted orbits is sparse in the vicinity: small perturbations typically drive the state into the attractor's basin. This is further evidence that Λ^0 and $\Lambda^{0,0}$ are attractors of ECA 18.

6.3 Subbasin decay

As we mentioned in Sec. 4, there is more than one possible choice of initial vicinity ensemble. The most obvious alternative to the Hamming vicinity V_H is the b_w-subbasin, denoted V_b, which contains all states with $w = 2$ dislocations on even-sized lattices and $w = 3$ on odd lattices. Clearly, $V_H \subset V_b$. The subbasin vicinity corresponds to the smallest "excitation" of the system, in the sense that the states have the minimal number of dislocations to move them off the attractor. In a parallel series of investigations on the same set of lattices as above, we calculated $f_P(t)$ for an initial ensemble of states drawn uniformly from b_2 or b_3, as appropriate. This induces a distribution of initial interdislocation distances that is uniform, rather than exponentially decaying, as was the case for V_H.

On all of the lattices measured, the convergence time T_c was the same for V_b as for V_H. On lattices where V_H had a vanishing asymptotic fraction f_P, V_b also gave $f_P = 0$. On the remaining lattices, f_P was typically higher for V_b than for V_H. Unlike the Hamming vicinity profiles, the even-size lattices did not follow a common backbone. Instead, they formed a family of similarly-shaped curves parametrized by the time-1 fraction $f_P(1)$. The time-1 fraction increased monotonically with lattice size to a limiting value. The profiles of the lattices fell into the same classification scheme as for V_H-decay, but the functional forms were different.

The stochastic model corresponding to the b_2-subbasin vicinity on a lattice of size N is a random mesa walker with a uniform distribution of interdislocation distances $d(0)$ on the interval $0 < d(0) \leq N/2$. The probability of a given site being occupied by a random walker is proportional to $1/N$, so that as N grows, relatively fewer random walkers fall off the cliffs in the first time-step. Numerical experiments showed that the time-1 fraction $f_{RMW}(1)$ varies with lattice size as $f_{RMW}(1) = c_1(1 - 1/N)$, with $c_1 = 0.25$. The observed decay curves quickly became exponential, $f_{RMW}(t) \sim 2^{-mt}$, and the decay rate m depended on lattice size as $m(N) = kN^{-\alpha}$, with $k = 16.0$ and $\alpha = 2.0$.

Finally, when a small amount of noise was added to the evolution of V_b, all lattices decayed to $f_P = 0$. All of the decay profiles for even-size lattices were approximately exponential, with a decay rate that decreased with increasing N. As for the RMW model, the decay rate on even-size lattices varied with lattice size roughly as $m(N) = kN^{-\alpha},\ \alpha \approx 2\,,\ k \approx 16$; the agreement with the RMW was better for larger N. Odd lattices decayed slightly faster than even lattices of corresponding size.

All of these results indicate that, while the functional forms of the V_b decay profiles differ in details from those of V_H, the convergence times, instability to perturbations, and overall classification scheme are preserved.

7 Concluding Remarks

Stepping back then, there are at present three general approaches to analyzing cellular automata: empirical studies using simulation, qualitative dynamics based on computation theory, and algebraic analysis. The preceding work attempted to bridge the gap between these alternative views by relating statistical behavior to the qualitative dynamics, and giving pointers to the relation of those two to the algebraic description. We investigated the diffusive behavior of dislocations as it controls the stability of ECA 18's attractors. The results indicate deviations that should reflect structures accessible via the algebraic analysis. The hope is that, despite the apparent spatio-temporal complexity exhibited by such simple models, much of the structure of nonlinear CA—especially those dominated by domains and walls—can be understood along these lines. At a minimum, though, the empirical results give a quantitative grounding to the actual frequency of occurrence of various phenomena. The earlier discussion [8] of the qualitative dynamics of ECA 18 left several questions unanswered. For example, how likely are deviations from the attractor-basin portrait? And, what fraction of vicinity patterns are not attracted back into the invariant set? The simulations presented here give the quantitative answers to these questions and the random mesa walker, an accurate phenomenological model.

Much of the deterministic CA's behavior is well-approximated as an ideal diffusion of a gas of annihilating dislocations. Thus, we interpret the deviations from the stochastic model of temporal decay into the attractor as being indicative of certain state space structures not captured by the attractor-basin portrait; these structures influence the decay on time scales set by the system size and boundary conditions. We found two major types of deviation: (i) final convergence in finite time to a nonzero fraction of states off the attractor; and (ii) systematic deviation by a roughly constant factor throughout the evolution. Both of these effects grow less pronounced as lattice size increases. The decay profiles themselves are closely related to the distribution of lengths of transients starting in the vicinity and falling into the attractor. We found that even-size lattices fall into two classes, one of which has a cutoff at short transient lengths, while for the other, much longer transients are present; odd-size lattices all showed long transients. For all lattices, there were many more short transients than long ones. The interesting observation is that the decay behavior for such a wide range of lattice sizes falls into so few classes. This is a result that is obscured in the discrete state space representation.

The asymptotic nonattracted fraction f_P measures the extent to which states fail to fall into the attractor. Our results show that, as a function of lattice size, the maximal values of f_P decrease as a power law. On very many lattices, especially large ones, f_P decays to 0. Thus in the limit of large N, the size of the nonattracted set goes to zero. A more detailed discussion of the lattice-size dependence of f_P must be left for presentation elsewhere.

In contrast to the deterministic CA, the decay profiles for noisy lattices indicate that the distinctions between the classes are destroyed by very small perturbations to the domains. All vicinity states collapse onto the attractor via a catastrophic decay whose features are captured by the random mesa walker. Thus even minimal noise washes out all deviations from the purely stochastic model. Asymptotically nonattracted orbits, and the state space structures supporting them, appear to exist only for perfectly noise-free evolution; they vanish if even the smallest amount of noise is present. And the latter, presumably, is the physically relevant context for the evolution of ECA 18.

The conclusion is that for moderate to large lattices, the Hamming and subbasin vicinities' nonattracted sets are both insignificant and unstable: Λ^0 and $\Lambda^{0,0}$ are regular attractors.

8 Acknowledgments

The authors wish to thank Dan Upper and Karl Young for helpful discussions, and the Beckman Institute and its Center for Complex Systems Research for their generous hospitality. This work was partially funded by ONR contract N00014-92-J-4024 and by a Visiting Research Professorship at the Beckman Institute, University of Illinois, Urbana-Champaign.

References

[1] P. Manneville. *Dissipative Structures and Weak Turbulence*. Academic Press, New York, 1990.

[2] B. Shraiman. Order, disorder and phase turbulence. *Phys. Rev. Lett.*, 57:325, 1986.

[3] M. Silber and E. Knobloch. Pattern selection in ferrofluids. *Physica*, D, 1988.

[4] A. R. Osborne, E. Segre, G. Boffetta, and L. Cavaleri. Soliton basis states in shallow-water ocean surface waves. *Phys. Rev. Lett.*, 67:592, 1991.

[5] W. I. Newman, D. K. Campbell, and J. M. Heyman. Identifying coherent structures in nonlinear wave propagation. *CHAOS*, 1:77, 1991.

[6] J. P. Crutchfield. Subbasins, portals, and mazes: Transients in high dimensions. *J. Nucl. Phys. B*, 5A:287, 1988.

[7] S. Wolfram. *Theory and Applications of Cellular Automata*. World Scientific Publishers, Singapore, 1986.

[8] J. E. Hanson and J. P. Crutchfield. The attractor-basin portrait of a cellular automaton. *J. Stat. Phys.*, 66:1415, 1992.

[9] P. Grassberger. Chaos and diffusion in deterministic cellular automata. *Physica D*, 10:52, 1984.

[10] K. Eloranta and E. Nummelin. The kink of cellular automaton rule 18 performs a random walk. Technical Report A296, Helsinki University of Technology, Institute of Mathematics, 1991.

[11] E. Jen. Aperiodicity in one-dimensional cellular automata. *Physica*, 44D:121, 1990.

[12] E. Jen. Exact solvability and quasiperiodicity of one-dimensional cellular automata. *Nonlinearity*, 4:251, 1990.

[13] D. R. J. Chillingworth. *Differential Topology with a View to Applications*. Pitman, London, 1976.

[14] J. Guckenheimer and P. Holmes. *Nonlinear Oscillations, Dynamical Systems, and Bifurcations of Vector Fields*. Springer-Verlag, New York, 1983.

[15] J. P. Crutchfield and J. E. Hanson. Turbulent pattern bases for cellular automata. In press, 1993.

[16] F. Spitzer. *Principles of Random Walk*. D. Van Nostrand Company, Princeton, 1964.

[17] W. Feller. *An Introduction to Probability Theory and its Applications*. John Wiley and Sons, New York, third edition, 1968.

[18] D. E. Knuth. *The Art of Computer Programming: Semi-Numerical Algorithms*, volume 2. Addison-Wesley, Reading, Massachusetts, second edition, 1981. problem 3.1.6.

[19] E. Jen. private communication.